scientific reports

Check for updates

OPEN

Physical and biogeochemical drivers of multi-year isoscape in the California upwelling system

Natasha L. Vokhshoori[1,2]✉, Genevieve Pugsley[2], Jerome Fiechter[2] & Matthew D. McCarthy[2]

Stable isotopes of carbon ($\delta^{13}C$) and nitrogen ($\delta^{15}N$) are commonly employed to reconstruct past change in marine ecosystems and nutrient cycling. However, multiple biogeochemical and physical drivers govern spatiotemporal variability of these isotopic signals, particularly in dynamic coastal systems, complicating interpretation. Here, we coupled a modern multi-year (2010–2019) $\delta^{13}C$ and $\delta^{15}N$ isoscape record from intertidal mussels (*Mytilus californianus*) with high-resolution ocean model output and satellite chlorophyll-a observations in the California Current System (32°–43° N) to identify major drivers of isotopic variability. Our results show that spatial variations in $\delta^{13}C$ are largely related to primary production, whereas spatial $\delta^{15}N$ variability is driven by water mass mixing. Major isotopic change was also related to ocean climate variability; however, these effects vary regionally. In northern and central California, $\delta^{15}N$ values are predominantly a function of nitrate utilization, whereas in southern California, $\delta^{15}N$ varies due to shifts in water mass composition. In all regions, $\delta^{13}C$ values are driven by productivity, with the largest changes occurring in southern California. Our findings provide novel insight into regional differences in predominant drivers of isotopic variability, and links to modern ocean climate variability. These findings offer crucial information needed for robust interpretations of California Current palaeoceanographic $\delta^{13}C$ and $\delta^{15}N$ records.

Keywords Carbon and nitrogen isotopes, Regional ocean circulation model, California current system

The California current system (CCS) is a dynamic eastern boundary current system characterized by strong, wind-driven upwelling which supplies cold, nutrient rich waters to the surface stimulating high primary production. The CCS extends between ~50° N to the north at the bifurcation of the North Pacific Current, and ~15–20° N to the south within the subtropical waters off Baja California, Mexico[1,2]. Variations in coastline morphology and upwelling intensity, among other environmental factors (e.g., river runoff, mixed layer depth, etc.), are known to affect biogeochemical cycles and physical ocean circulation through space and time along the US west coast[3,4]. The CCS can be grouped into three distinct subregions based on characteristic patterns of alongshore wind intensity and seasonality, and therefore upwelling dynamics[5]. From Cape Mendocino northward (40–50° N), winds are moderately strong and seasonally variable, blowing equatorward in the spring and summer months and reversing direction in the fall and winter months. In the central CCS between Pt. Conception and Cape Mendocino (34.5–40° N) winds are stronger and more predominantly upwelling favorable. In the Southern California Bight south of Pt. Conception (32–34.5° N), winds are relatively weak year-round and persistently equatorward. Interannual and decadal ocean climate variability associated with the El Niño Southern Oscillation (ENSO)[6], Pacific Decadal Oscillation (PDO)[7], and North Pacific Gyre Oscillation (NPGO)[8] can strongly affect sea surface temperature (SST), upwelling intensity, water mass composition, and nutrient availability throughout the CCS. In general, over the past several decades, El Niño events (i.e., above average SST, increased stratification, and weakened upwelling) coincide with positive phases of the PDO[9] and, since 1999, negative phases of NPGO[8].

Isotope spatial gradients, or *isoscapes*, have the power to characterize variable biogeochemical regimes across an ecosystem or region[10]. Although isoscapes constructed using isotopic values of primary producers most closely represent the base of the food web[11,12], marine phytoplankton are short-lived with relatively noisy isotopic signatures, leading to poor representation of interannual variability. In contrast, isoscapes constructed from a primary consumer are more representative of annually integrated signals[13–16].

Factors affecting $\delta^{13}C$ values in marine primary productivity include growth rate, cell size and cellular uptake of carbonate species with distinctive $\delta^{13}C$ values[17]. In general, all these mechanisms work together to promote higher $\delta^{13}C$ values of primary production when primary production and nutrient supply are high. High nutrient availability promotes rapid growth of relatively large-celled phytoplankton taxa, leading to higher

[1]Geology Department, St. Lawrence University, Canton, NY, USA. [2]Ocean Sciences Department, University of California, Santa Cruz, Santa Cruz, CA, USA. ✉email: nvokhshoori@stlawu.edu

$\delta^{13}C$ values. Additionally, since bicarbonate has a much higher $\delta^{13}C$ value (0 to 2.4‰) than atmospheric CO_2 (−8‰)[18], utilization of bicarbonate rather than CO_2 can dramatically increase $\delta^{13}C$ values of primary production. Light limitation and nutrient repletion, both of which are common in upwelling regions with high turbulence, biomass accumulation and nutrient availability, can also lead to higher $\delta^{13}C$ values by influencing intracellular carbon concentrating mechanisms[19]. In all, these factors affect how mussels record primary production and/or phytoplankton community structure.

For $\delta^{15}N$, two different mechanisms are likely the primary controls on $\delta^{15}N$ isoscapes and variability through time: circulation of water masses with distinct nitrate $\delta^{15}N$ signatures and nitrate utilization variability. Disentangling the roles of water mass circulation and nutrient utilization can be especially challenging when interpreting palaeoceanographic $\delta^{15}N$ records, and we aim to elucidate which of these processes are important drivers of variability in different regions of the CCS. The CCS is a dynamic oceanographic region where several water masses with distinct salinity, temperature and nutrient profiles mix. The two major water masses in the CCS are Pacific Equatorial Water (PEW) which is warmer, saltier and has higher nitrate concentrations, and Pacific Subarctic Upper Water (PSUW) with a cooler, fresher and lower nitrate concentration profile[20]. In PEW, nitrate is relatively enriched in $\delta^{15}N$ (~14–16‰) because it originates from the eastern tropical North Pacific, where low oxygen concentrations drive strong water-column denitrification[21]. In contrast, PSUW represents open ocean $\delta^{15}N\text{-}NO_3^-$ values of ~4–5‰[22]. A strong latitudinal gradient associated with alongshore mixing in the CCS of these two water masses was initially observed in water column nitrate and sinking particles[23] and later found to be also recorded in mussels[14]. PSUW is advected equatorward by the California Current, the eastern boundary current of the North Pacific subtropical gyre, whereas PEW is transported poleward by the California Undercurrent, a subsurface current (100–500 m) that contributes to upwelled source waters. Additionally, variations in nutrient utilization likely exert an important control on $\delta^{15}N$ values in some regions. Incomplete nitrate utilization in the nearshore CCS is common, particularly in the central and northern regions, due to iron limitation and rapid offshore advection of nutrients before they can be fully utilized by phytoplankton[24,25]. Phytoplankton preferentially incorporate nitrate containing the light stable isotope of nitrogen[14], N, leading to isotopic depletion of phytoplankton biomass relative to source nitrate when utilization is incomplete[26]. Finally, mussel physiology may affect $\delta^{13}C$ and $\delta^{15}N$ values in extreme cases of thermal stress where higher respiration/oxidative stress causes an accumulation of the heavy ^{13}C (and ^{15}N) isotope resulting in higher $\delta^{13}C$ values (and $\delta^{15}N$ values)[27,28]. This is because glycogen, the energy stores in mussel tissues, drop significantly under exposure to high temperatures[29]. These associated effects are akin to mussels that inhabit the high tidal zone of the intertidal zones which experience more temperature extremes and typically have higher $\delta^{13}C$ values compared to mid and low tide mussels[30] but also may be more reflective of future ocean conditions.

In the CCS, determining the physical and biogeochemical controls on isotope values is difficult because of multiple interrelated factors that vary latitudinally (e.g., upwelling strength, coastline morphology, temperature, nitrate supply, etc.). Isotope proxies measured from paleo-archives such as sediments, coral, and other calcifying organisms (e.g., bivalves and gastropods) to reconstruct past change in CCS biogeochemistry, are in need for robust interpretational frameworks to link past isotopic variability with meaningful ecosystem parameters. Moreover, little is known about what the driving mechanisms of these biogeochemical regimes are with interannual climatic oscillations, or how they will change with anthropogenically induced climate warming.

Here, we combine a 7-year record of California isoscapes (between 2010 and 2019) with a high-resolution biophysical model to identify the main physical and biogeochemical mechanisms driving $\delta^{13}C$ and $\delta^{15}N$ signatures in the California Current System. Spatial and interannual oceanographic and biogeochemical variability is characterized using simulated ocean temperature, nitrate concentrations and upwelling, as well as satellite chlorophyll-a observations and climate indices (PDO, NPGO, ENSO), and directly compared to corresponding isotopic data. With this work, we aim to address the following questions: (1) What are the primary physical–biogeochemical drivers controlling $\delta^{13}C$ and $\delta^{15}N$ values in the three major latitudinal regions of the CCS? and (2) How are $\delta^{13}C$ and $\delta^{15}N$ related to ocean climate variability, such as ENSO, PDO and NPGO? These questions are important for better calibrations of geochemical paleo-proxies for historical reconstructions of California isoscapes as well as predicting future climate warming impacts at a regional scale.

Results

Carbon and nitrogen isotope results

Carbon isotope values ($\delta^{13}C$) measured in the adductor muscle tissue of California Mussel (*Mytilus californianus*), between 2010 and 2019 for all sampling sites (32°–42°N) ranged between −19.0‰ and −14.0‰ (Fig. 1, Table S1). Sampling year 2010 had on average the highest $\delta^{13}C$ values (−15.7‰ ± 0.9) while 2016 had the lowest (−17.0‰ ± 1.0). A Welch two-sample t-test showed that the difference between these two years was statistically significant, $t(43.67) = 4.73$, $p < 0.0001$. There was no latitudinal trend with $\delta^{13}C$ values for any of the years except in 2016 (mean all years: $y = 0.032x - 17.62$, $r^2 = 0.04$, $P > 0.05$; 2016: $y = 0.22x - 25.21$, $r^2 = 0.51$, $P = 0.0002$).

Nitrogen isotope values ($\delta^{15}N$) for all years and sampling sites ranged between ~7‰ to 12‰ (Fig. 1). Sampling years 2011 and 2019 had on average the lowest $\delta^{15}N$ values (9.5‰ ± 0.9-1.0) and 2016 had the highest $\delta^{15}N$ values (10.3 ± 0.8). In contrast to the $\delta^{13}C$ time series isoscape, all years showed a significant negative linear trend with latitude (mean all years: $y = -0.21x + 17.65$, $r^2 = 0.61$, $P > 0.00001$), however 2016 had the weakest latitudinal trend ($y = -0.11x + 14.4$, $r^2 = 0.19$, $P = 0.432$).

In our isotope records, the years 2010 and 2016 stand out, displaying especially anomalous $\delta^{15}N$ and $\delta^{13}C$ values in some regions (Fig. 2). $\delta^{15}N$ values in the central and northern part of the California Current were 0.5 to 1.0‰ higher than the average in 2016. Conversely, $\delta^{13}C$ values in 2016 were anomalously low in the south, −1 to −1.5‰ lower, than the average. In 2010, $\delta^{13}C$ values were in general higher in all regions of the CCS, especially at the more southern locations.

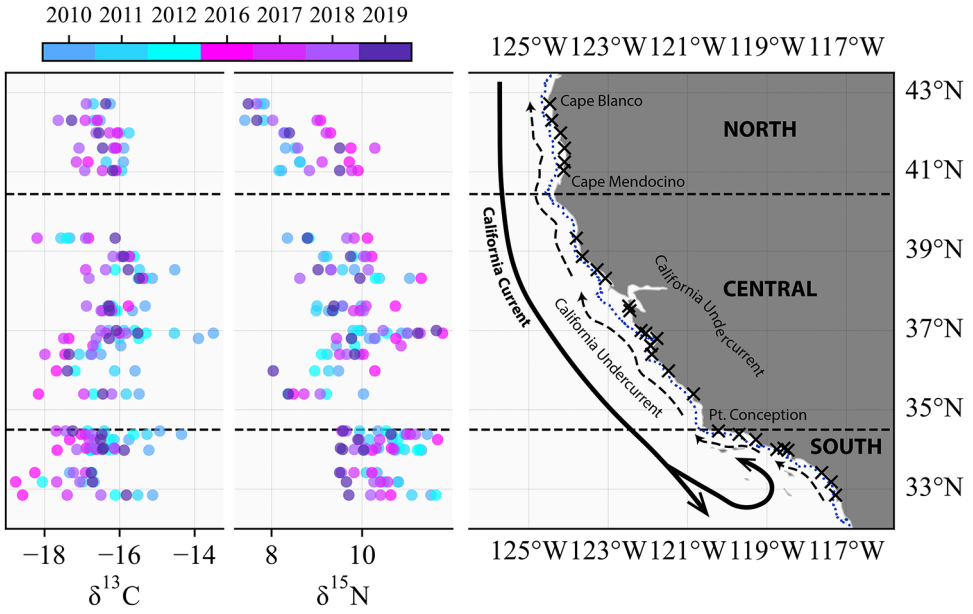

Fig. 1. Site-specific bulk $\delta^{15}N$ and $\delta^{13}C$ values measured in soft tissue of *Mytilus californianus* as a function of latitude and sampling years (colored circles) in context of a map of collection sites on the California coast (X symbol) with the dotted line (blue) following the coast is the 100 m isobath. Major regions, currents and key geographic landmarks are shown: the horizontal dashed lines indicate the regions northern (40–43° N), central (34.5–40° N) and southern (32–34.5° N) CCS subregions; ocean currents: California Current (solid) and California Undercurrent (dashed) adapted from Checkley and Barth[5]. The equatorward moving California Current advects PSUW originating in the northern subarctic while the poleward moving California Undercurrent advects PEW that originates in the equatorial pacific (see Bograd et al.[20]).

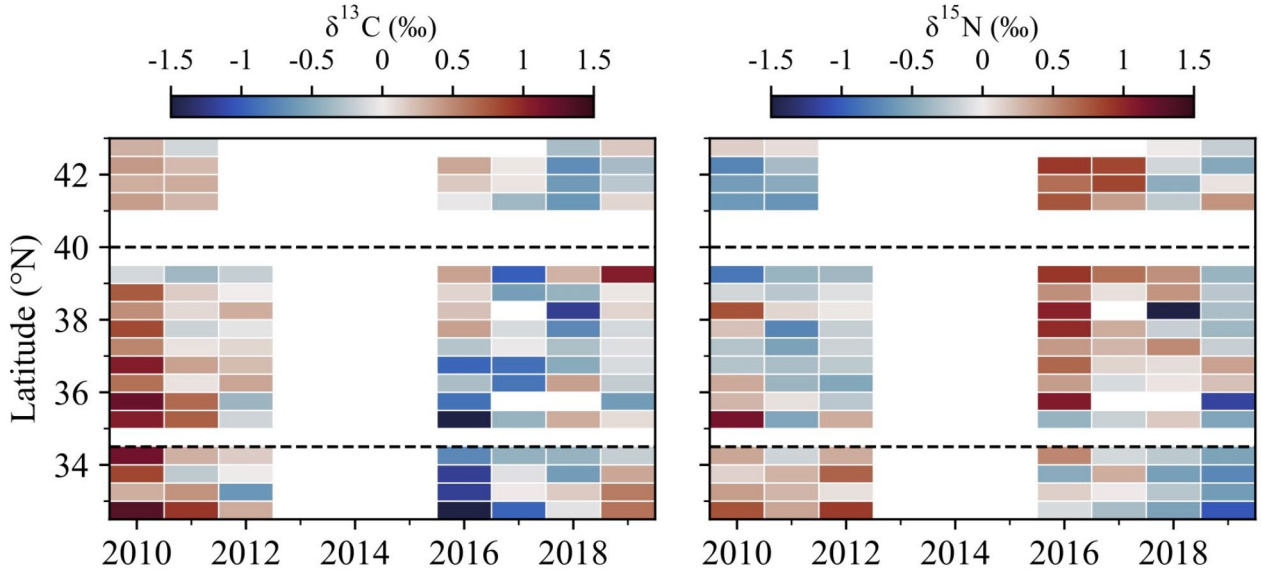

Fig. 2. Bulk $\delta^{13}C$ and $\delta^{15}N$ anomalies measured in soft tissue of *Mytilus californianus* binned by 0.5 degree latitude and sampling year. Horizontal dashed lines separate the northern (40–43° N), central (34.5–40° N) and southern (32–34.5° N) CCS subregions.

Model output and satellite chlorophyll-a

Over the duration of our record, satellite chlorophyll-a and simulated nitrate and upwelling intensity display considerable interannual variability (Fig. 3). Chl-a and upwelling velocity anomalies display relatively high-frequency variability and low spatial coherence. In contrast, nitrate and temperature anomalies are spatially

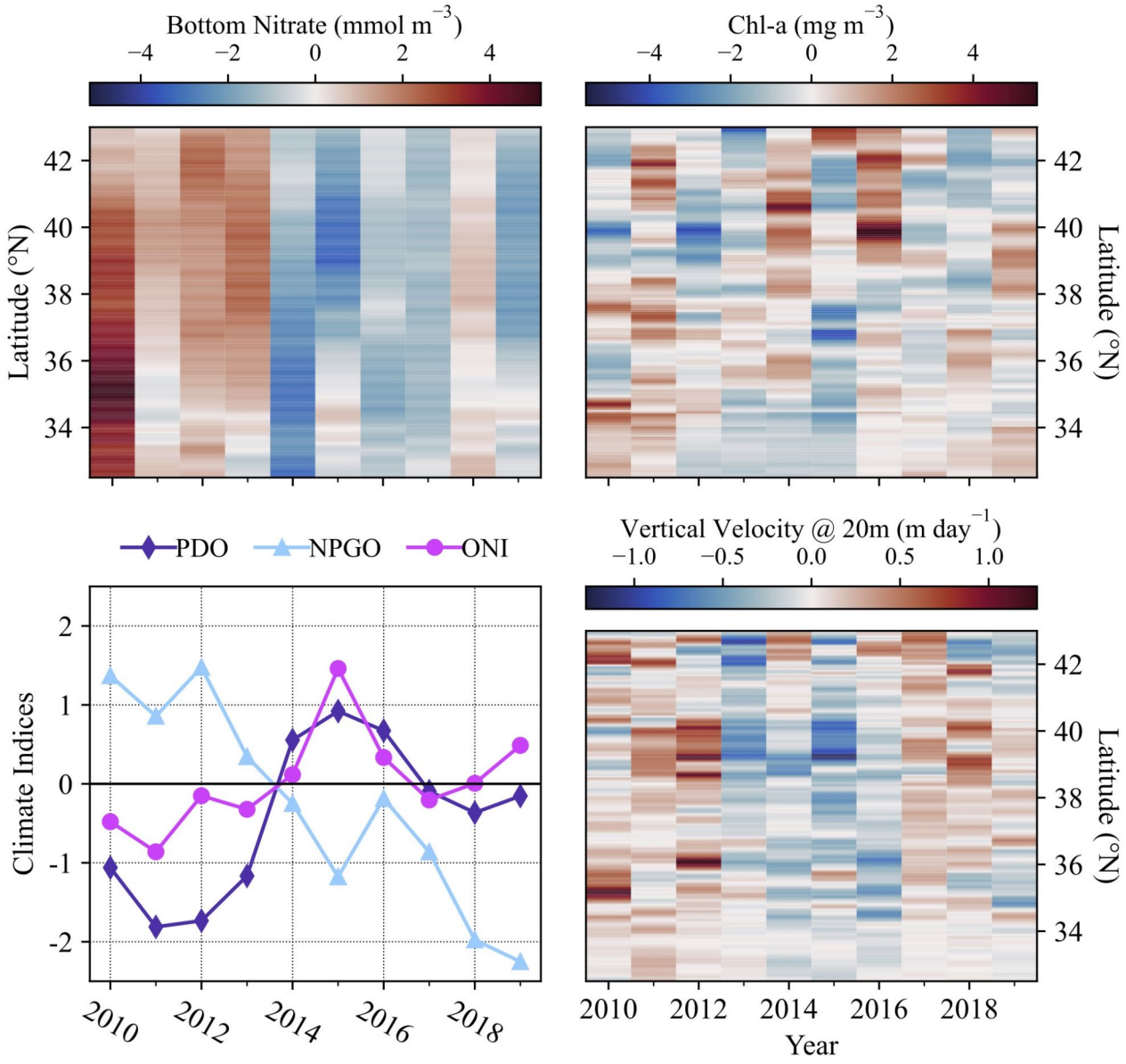

Fig. 3. Oceanographic data anomalies (bottom nitrate, mmol m^{-3}; Chlorophyll-a, mg m^{-3}; vertical velocity at 20-m depth, m day^{-1}) and climate index anomalies (*PDO* Pacific Decadal Oscillation, purple diamonds, *NPGO* North Pacific Gyre Oscillation, blue triangles, *ONI* Oceanic Niño Index, pink circles) for sampling period (2010–2019) and latitudinal range (32° N–43° N).

coherent across latitude and coincide with shifts in the phases of the PDO, NPGO and ONI. (Fig. 3, Fig. S1). For example, there is a clear shift between 2013 and 2014 from high nitrate concentrations and low temperatures to low nitrate concentrations and higher temperatures at all latitudes. This sharp transition aligns with striking shifts in the NPGO (positive to negative), PDO (negative to positive) and Oceanic Niño Index (ONI) (neutral to positive). Other noteworthy features in the physical and biogeochemical data are weakened upwelling in 2015 and 2016, and exceptionally high Chl-a in the northern part of the CCS during this same time period related to the extreme 2014-2016 marine heatwave[31].

Relationships between oceanographic and isotopic variability

In our analysis of spatial variability, PC1 and PC2 explained 87.2% of total variance in the oceanographic variables (Fig. 4; Table 1). PC1 was most strongly correlated with latitude, surface temperature and bottom nitrate, and explained 69.7% of the total variance. $\delta^{15}N$ values significantly correlated with PC1 (Spearman's $\rho = 0.73$; $p < 0.001$), but $\delta^{13}C$ values did not. The strongest loadings for PC2 were shelf width, upwelling, and Chl-a and it explained 17.5% of the total variance. $\delta^{13}C$ significantly correlated with PC2 (Spearman's $\rho = 0.37$, $p = 0.05$), but $\delta^{15}N$ did not.

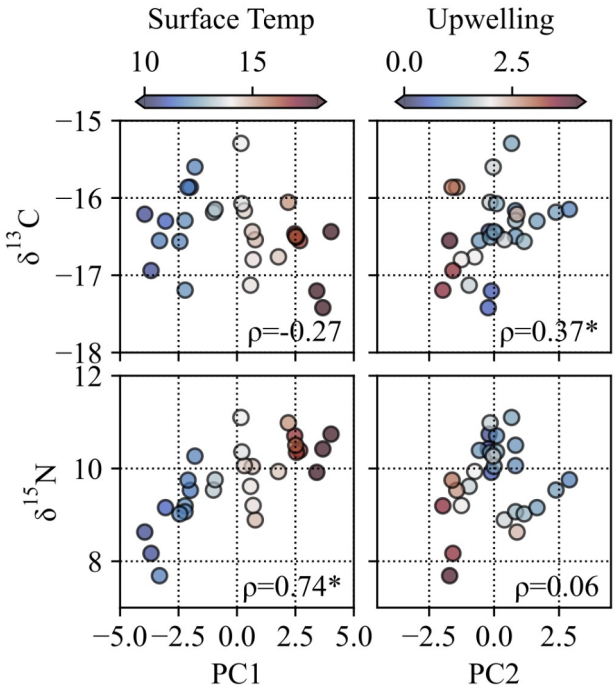

Fig. 4. Analysis of spatial variation of $\delta^{13}C$ and $\delta^{15}N$ values described by Principal Components 1 and 2. Each dot represents the average of all sampling years for each sampling site. Color shading is based on the most explanatory dynamically varying variable (not geographically constrained like latitude and shelf-width) for each respective principal component: surface temperature (°C) for PC1 and upwelling for PC2. Spearman's rho values with an asterisk indicate statistical significance ($p < 0.05$).

	PC1	PC2
Bottom nitrate	− 0.98	− 0.05
Surface nitrate	− 0.90	− 0.10
Bottom temperature	0.92	0.20
Surface temperature	0.99	0.02
Upwelling	− 0.70	− 0.65
Chl-a	− 0.71	0.58
Shelf width	− 0.46	0.80
Latitude	− 0.99	0.00
Variance explained	69.7	17.5

Table 1. Principal component analysis loadings for spatial means.

Due to variable isotopic responses to oceanographic forcing in different regions of the CCS, correlations between isotopic variables and the temporal PCA amplitudes were calculated separately for each subregion (i.e., northern (40.5–43° N), central (34.5–40.5° N) and southern (32-34.5° N) CCS. In our analysis of temporal anomalies relative to the mean at each study site, PC1 and PC2 explained 77.8% of total interannual variance in the oceanographic variables (Fig. 5; Table 2). PC1 explained 59.2% of the total variance, and the strongest loadings were bottom nitrate and surface temperature. PC2 was most strongly correlated with Chl-a followed by upwelling, and it explained 18.6% of the total variance. $\delta^{13}C$ anomalies positively correlated with PC1 in all three subregions (Spearman's $\rho = 0.61$, 0.39 and 0.58 in the north, central and southern regions, respectively, $p < 0.001$ for all regions). While $\delta^{15}N$ anomalies were also significantly correlated with PC1 in all three subregions, the direction of the relationship varies regionally. At southern latitudes, the correlation is positive (Spearman's $\rho = 0.45$, $p < 0.001$), and at central and northern latitudes, the correlations are negative (Spearman's $\rho = -0.23$, $p = 0.04$ and Spearman's $\rho = -0.55$, $p < 0.001$, respectively). $\delta^{13}C$ anomalies exhibited a negative relationship with PC2 in all regions, which is statistically significant in southern (Spearman's $\rho = -0.43$, $p < 0.001$) and central (Spearman's $\rho = -0.28$, $p = 0.01$) subregions. $\delta^{15}N$ anomalies did not correlate with PC2 in any of the three regions.

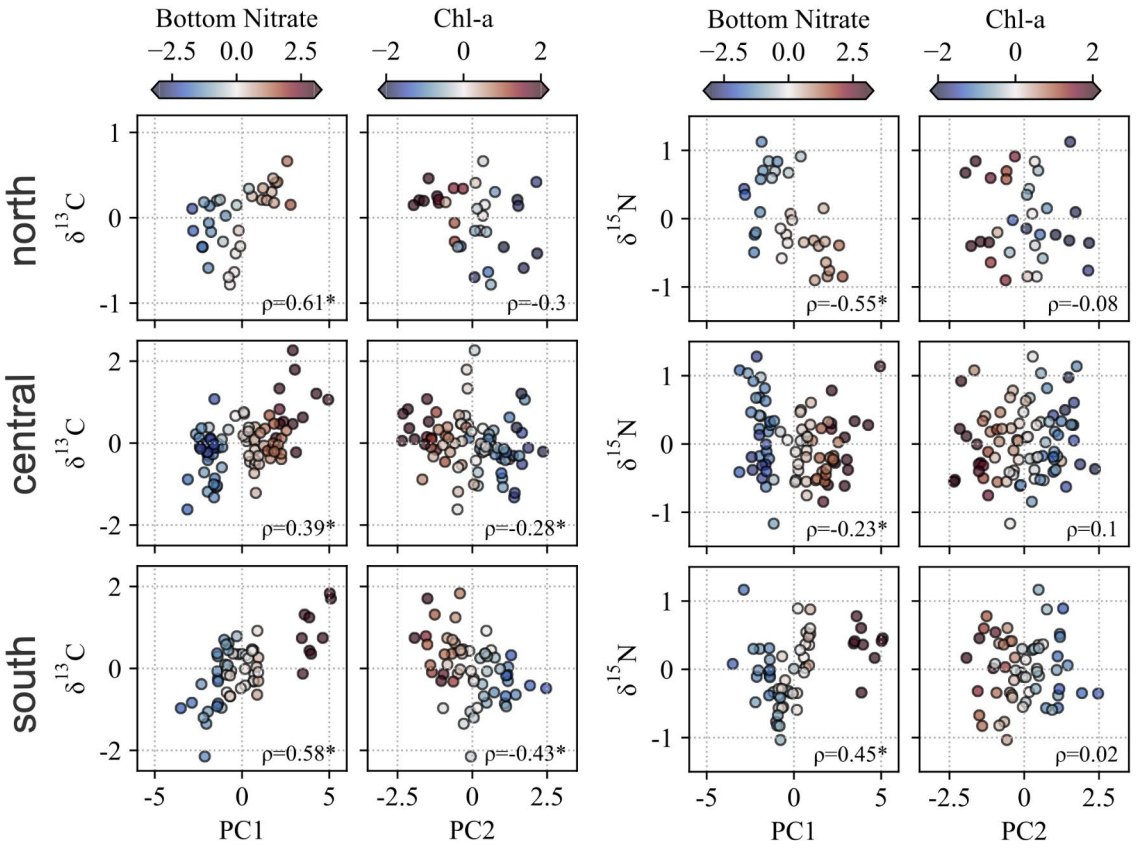

Fig. 5. Analysis of temporal variation of $\delta^{13}C$ and $\delta^{15}N$ anomalies described by Principal Components 1 and 2 for the northern (40–43° N), central (34.5–40° N) and south (32–34.5° N) subregions (from top to bottom). Each dot represents the isotope anomaly from a specific sampling site and year. Color gradient is based on the most explanatory variable for each respective principal component: bottom nitrate for PC1 and Chlorophyll-a for PC2. Spearman's rho values with an asterisk indicate significance.

	PC1	PC2
Bottom nitrate	0.94	0.01
Surface nitrate	0.87	− 0.18
Bottom temperature	− 0.91	− 0.15
Surface temperature	− 0.94	0.11
Upwelling	0.46	0.48
Chl-a	0.13	− 0.91
Variance explained	0.59	0.19

Table 2. Principal component analysis loadings for temporal anomalies.

Relationships between basin-scale climate modes and isotopic variability

We find strong relationships between the California Current mussel isotope records and basin-scale modes of climate variability (PDO, NPGO and ENSO) based on Spearman correlation coefficients (Fig. 6). $\delta^{13}C$ is negatively correlated with PDO and ONI, and positively correlated with NPGO in all regions. In the southern region, only $\delta^{13}C$ relationships with PDO and ONI are significant. In the northern region, only relationships with NPGO and ONI are significant. Correlations with $\delta^{15}N$ vary regionally, with positive relationships to PDO and ONI occurring in the northern and central (although weaker) subregions, and negative relationships in

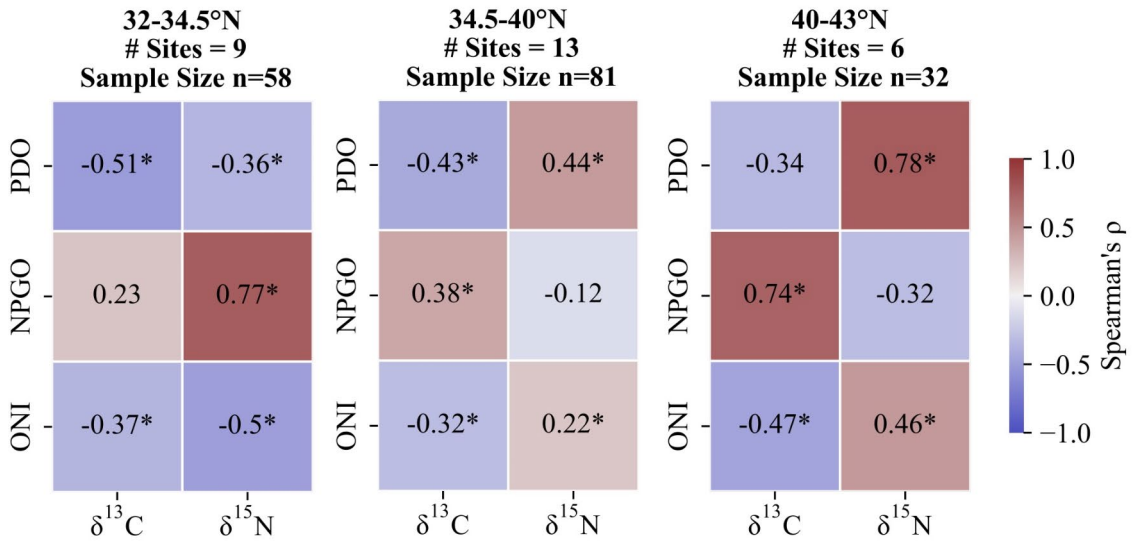

Fig. 6. Spearman Correlations between oceanic oscillation variables and isotopes by subregion: southern (32–34.5° N), central (34.5–40° N) and northern (40–43° N). Rho values with an asterisk indicate significance.

the southern subregion. As expected, relationships between NPGO and $\delta^{15}N$ had the opposite sign as PDO and ONI[8], with negative correlations in the northern and central subregions, and a positive correlation in the southern subregion. In the central and northern subregions, only relationships with $\delta^{15}N$ and PDO and ONI are significant.

Discussion

Drivers of spatial isotopic variability in the CCS

The spatial variations in $\delta^{15}N$ we observe are consistent with known latitudinal changes in dominant water masses with characteristic nitrate $\delta^{15}N$ signatures. We find a decreasing trend in $\delta^{15}N$ values with latitude (Fig. 1) in all years except 2016, which was affected by the strong 2015–2016 El Niño event (Figs. 2, 3). In our PCA analysis, spatial variations in $\delta^{15}N$ were strongly correlated with PC1, which reflects predominantly latitudinal variations in nitrate concentrations and temperature (Fig. 4). We postulate here that temperature and nitrate concentrations are not the direct cause for variations in $\delta^{15}N$ values, but rather that these variables represent latitudinal differences in water mass composition driven by the regional ocean circulation. The progressive decrease from higher $\delta^{15}N$ values in southern California to lower values at the more northern latitudes (Fig. 1) likely results from greater contributions from PEW with high nitrate $\delta^{15}N$ signatures in the southern part of the domain and increasing contribution of PSUW with lower nitrate $\delta^{15}N$ signatures in the northern part of the domain. Based on a similar implementation of the ROMS-NEMUCSC model, Fiechter and Moore[32] report a decrease in PEW fraction in upwelled source waters from ~45% at 35° N to ~25% at 43° N.

We found our results to be consistent with primary production as a major driver of $\delta^{13}C$ spatial variability. Supporting this argument is the strong positive correlation between satellite chlorophyll-a and $\delta^{13}C$ values (Fig. S4), and in the spatial PCA analysis, PC2 was the strongest predictor for $\delta^{13}C$ (Fig. 4). The oceanographic variables with the strongest loadings on PC2 are shelf width, Chl-a and upwelling. The loadings (Table 1) suggest that $\delta^{13}C$ is positively related to Chl-a and shelf width, and negatively related to upwelling. These findings align with past work in the CCS that have examined spatial variability in primary production. Enhanced primary production occurs "downstream" of major upwelling centers in the CCS[4]. In the spatial PCA analysis, the negative loading of upwelling and positive loading of Chl-a on PC2 suggests local "hotspots" of high primary production occurs in areas of low upwelling, once large-scale latitudinal gradients in upwelling and productivity (as represented by PC1) are accounted for. In the CCS, local sites of strong upwelling occur near prominent topographic features such as around Cape Blanco (~43° N), Cape Mendocino (40° N), Point Arena (39° N), Point Año Nuevo (37° N), Point Sur (~36° N) and Pt. Conception (34.4° N) (see Fig. 1). Alongshore advection carries upwelled nutrients to adjacent regions, creating productivity "hotspots" that are spatially decoupled from the locations where upwelling is most intense[3,4].

Taking a closer look at the spatial $\delta^{13}C$ patterns in our dataset, we see that there is strong agreement between previously proposed productivity "hotspots" and areas of high $\delta^{13}C$ values, such as our sampling sites at 38° N

south of Point Arena (− 15.6 ± 0.6) and Santa Barbara just south of Pt Conception (34.4° N; − 16.1 ± 0.9) (Fig. 1, Fig. S4). The northern tip of the Monterey Bay south of Point Año Nuevo had on average the highest $\delta^{13}C$ values across all sampling sites and years (37° N; − 15.3 ± 1.0), even though it is not where the highest chlorophyll concentrations are found. This is probably because Monterey Bay is uniquely in an "upwelling shadow". Point Año Nuevo is a persistent upwelling center, and plumes of cool, saline, nutrient-rich water are advected into Monterey Bay[33,34]. When these waters mix with the warmer, more protected waters in the northern part of the bay[35], it fosters dense phytoplankton blooms[36].

Other factors we suggest our $\delta^{13}C$ data is recording are aligned with past work that indicate both Shelf Width and Chl-a increase with latitude in the CCS[37], likely due to the effects of river discharge and shelf width on iron limitation. Fluvial sediments are the primary source of iron to coastal waters. Areas of high sediment discharge also develop broad continental shelves with gradual slopes, which retain iron and enhance delivery of iron-rich bottom boundary layer waters to the surface, enhancing productivity[24,38,39]. Our data broadly corroborate this argument: we see positive relationships between shelf width and Chl-a, and both variables positively correlate with latitude (Fig. S2); although our $\delta^{13}C$ multi-year isoscape record does not exhibit a latitudinal trend (except in 2016), likely because of the overprinting of the aforementioned productivity "hotspots". Finally, there are other possible site-specific differences affecting $\delta^{13}C$ values that were not accounted for in our analysis, such as coastal environment type (i.e., beach vs. jetty vs. rocky intertidal), phytoplankton community structure (i.e., diatom vs. dinoflagellate vs. bacteria) sea bottom redox conditions (i.e., local water column denitrification) and potentially pH. Our spatial and temporal analyses explain 87.2% and 77.2% of the total variability however there is a chance some of the variability is caused by factors not included in our analysis.

Drivers of temporal isotopic variability in the CCS

Our analyses of temporal variability indicate that both carbon and nitrogen isotope signatures are associated with climate-driven interannual variations in temperature and nutrient availability. However, we find important regional differences in drivers of $\delta^{15}N$ variability as well. In all three regions, both carbon and nitrogen isotope anomalies were correlated with temporal PC1, which had strong loadings on simulated temperature and nitrate concentrations. In addition, PC2, which is most strongly related to chlorophyll-a, was an important predictor for $\delta^{13}C$ values. Directional relationships between oceanographic predictors and $\delta^{13}C$ values were consistent across all regions of the CCS and are consistent with nutrient supply and primary production as major drivers of $\delta^{13}C$ interannual variability. In contrast, the direction of relationships between oceanographic variables and $\delta^{15}N$ values were different in the southern compared to the central and northern regions, although central California showed a much weaker relationship likely related to the transition from non-upwelling dominated zones in southern parts of the Central coast (e.g. Big Sur) to stronger upwelling dominated zones further north (e.g. Monterey and Pt. Arena) (Fig. S5). In the southern subregion, $\delta^{15}N$ values positively correlated with PC1 (associated with high nitrate and low temperature), whereas in the central and northern subregions, $\delta^{15}N$ values negatively correlated with PC1. It is also interesting to note that upwelling was positively coupled with $\delta^{15}N$ values in the southern subregion but negatively coupled in the central and northern subregions (Fig. S3). Therefore, at southern latitudes, $\delta^{15}N$ values *increase* with higher upwelling and bottom nitrate concentrations, whereas at central and northern latitudes, $\delta^{15}N$ values *decrease*.

Together, we suggest that central and northern California $\delta^{15}N$ values are most strongly driven by changes in nitrate utilization. Incomplete utilization of the nitrate pool by phytoplankton is common in the nearshore central and northern subregions[25] and leads to lower $\delta^{15}N$ values of primary production compared to source water nitrate. Therefore, we would expect higher $\delta^{15}N$ values when nutrient utilization is more complete, such as when upwelled nutrient supply is lower and when upwelled waters are retained in the nearshore region for longer, facilitating more complete utilization by phytoplankton. This hypothesis is consistent with our findings for central and northern California, where we find evidence for higher $\delta^{15}N$ values of primary production in years when upwelling is less intense and nutrient concentrations lower.

Conversely, we postulate that interannual $\delta^{15}N$ variability in the southern subregion is driven primarily by variations in the contribution of PEW to the water masses reaching the euphotic zone, as suggested by the increase in $\delta^{15}N$ values when upwelling and nitrate concentrations increased. Since this finding is *inconsistent* with nutrient utilization as the primary mechanism driving $\delta^{15}N$ variability, the interannual variability of $\delta^{15}N$ values in the southern subregion presumably represent that of upwelled source waters. Bograd et al.[20] found increased contributions of PEW to the Southern California Bight euphotic zone during periods of reduced stratification, enhanced upwelling and deeper upwelling source depths which typically occurs during La Niña events; while PEW is typically found much deeper below the thermocline (300–500 m) during El Niño events. Our findings agree with their results and suggest that interactions between upwelling and water mass composition may play an important role in driving $\delta^{15}N$ values in modern and paleo-archives from the Southern California Bight[14].

Relationships between climate regime change and isotopic variability

Across our 7-year record, much of the temporal isotopic variability can be explained by major shifts in oceanographic variables (e.g., upwelling intensity, nutrient concentrations, and satellite chlorophyll-a) coinciding with changes in ocean climate conditions tied to the El Niño Southern Oscillation, Pacific Decadal Oscillation and North Pacific Gyre Oscillation (Figs. 3, 6). The most notable climate "extremes" in our sampling record were in 2010 when the PDO was reached its highest negative value and the NPGO its highest positive value, and later in 2016 with the 2015-2016 El Niño being one of the strongest on record[40].

The strongly negative PDO conditions in 2010 coincided with lower SST, stronger upwelling, and the highest simulated bottom nitrate concentrations over the 10-year period, especially in the southern subregion (Fig. 3). $\delta^{13}C$ values were on average highest in 2010 compared to the rest of our sampling record, indicating higher primary productivity in all subregions (Fig. 2). Our $\delta^{15}N$ record demonstrates the strongest latitudinal gradient

in 2010, with the lowest recorded $\delta^{15}N$ values in the northern subregion, and the highest values recorded in the southern subregion (Fig. 1). As explained in "Drivers of temporal isotopic variability in the CCS" section, this finding is consistent with the fact that the northern subregion is primarily driven by nitrate utilization processes, whereas in the southern subregion, source water $\delta^{15}N$ values are the primary driver (i.e., PEW advected from the south has a distinctly elevated $\delta^{15}N$ nitrate signal).

During the positive PDO and ONI conditions of 2016, upwelling and bottom nitrate concentrations were relatively low (Fig. 3), and we documented the lowest $\delta^{13}C$ values on record, driven mostly by especially low $\delta^{13}C$ values in the southern part of the domain. Primary production, represented by Chl-a (Fig. 3), was also lowest in the southern subregion in 2016 compared to all other years (Fig. 3) and clearly explains why $\delta^{13}C$ values were lowest there during that time. In contrast, the average highest $\delta^{15}N$ values were recorded in 2016, primarily driven by anomalously high values in the northern part of the domain (Fig. 2). Even though bottom nitrate concentrations were at or below average in the northern subregion in 2016, Chl-a concentrations were the highest, especially in the vicinity of Cape Mendocino (40° N). The 2015-2016 El Niño event coincided with the most extreme 2014-2016 marine heatwave ever recorded in the CCS spanning the entire eastern Pacific from the Aleutian Islands to the southern tip of Baja California and caused the largest harmful algal blooms on record in northern and central California[31,41]. The diatom *Pseudo-nitzschia* which produces the neurotoxin Domoic Acid, closed many commercial and recreational shellfish and fin fisheries and caused many marine mammal strandings along the U.S. West Coast. Elevated levels of the toxin were recorded in shellfish including mussels and razor clams from Vancouver Island to Central California[31]. Though toxic, the high algal concentrations due to a series of factors—upwelling, storms and anomalously high SST—meant that the phytoplankton consumed all the available nitrate. As a result, high nitrate utilization increased $\delta^{15}N$ values in response. Overall, we found that the PDO and ONI most significantly related to $\delta^{15}N$ values in the northern and central subregions and to $\delta^{13}C$ values in the southern subregion. While our sampling record is relatively short compared to these interannual and decadal modes of climate variability, the connections established here contribute to an improved understanding of the impact of basin-scale processes and oceanic regime shifts on carbon and nitrogen isotope variability in palaeoceanographic records.

Conclusions

Geochemists and paleoceanographers have been challenged with decoding physical and biogeochemical drivers of stable isotope proxies in marine systems. Moreover, these drivers are often assumed to be constant across broad regional scales. In heterogenous systems such as eastern boundary current upwelling regions, this can pose a problem since physical and biogeochemical processes will substantially vary by latitude in response to differences in coastline morphology, proximity to riverine outflows, and with cyclic or stochastic environmental perturbations. By combining a temporal record of measured $\delta^{13}C$ and $\delta^{15}N$ values from a base level consumer with output from a high-resolution biophysical ocean model, our approach allows for a more diagnostic characterization of processes driving variation in isotope records that would otherwise be difficult to deconvolve from a spatial record alone. In this study, we investigated physical and biogeochemical drivers of carbon and nitrogen isotope variability in one of the most studied regions in the world's oceans, the California Current upwelling system. We found that the dominant driver of $\delta^{13}C$ spatiotemporal variability is primary production controlled by shelf width and site-specific productivity "hot spots" adjacent to known regions of intensified upwelling. In contrast, drivers of $\delta^{15}N$ values differed by region: at central and northern latitudes, $\delta^{15}N$ is primarily controlled by the extent of nitrate utilization, whereas at southern latitudes, $\delta^{15}N$ values are primarily controlled by water mass composition. While both mechanisms affect $\delta^{15}N$ values, this study shows the predominant driving mechanism to be different in the northern subregion versus the southern subregion. These results have major implications for palaeoceanographic studies that analyze organic $\delta^{13}C$ and $\delta^{15}N$ isotopes in a variety of paleo-archives including sediment cores, ancient and living deep-sea corals, and shelly remains of calcite-bearing organisms such as bivalves and gastropods as well as understanding how interannual climatic oscillations, will change with future climate warming.

Materials and methods

Sample collection and processing

California mussels (*Mytilus californianus*) were collected from 28 different sites between Coos Bay, Oregon (42° N), and San Diego, California (32° N), in the winter (Dec–Feb) of 2009/2010, and summer (Jun.–Jul/Aug.) of 2011, 2012, 2016, 2017, 2018 and 2019 (Fig. 1). Sites were chosen to be approximately evenly distributed along the CA coastline, with ~80 km geographic separation. Typically, 5 mussels were collected from each site, between 40- and 60-mm maximum shell length, and were immediately preserved on dry ice until further preparation. The adductor muscle of each individual was dissected for analysis. This tissue was selected because feeding experiments and seasonal sampling studies have shown that the isotopic turnover rate of adductor tissue of this size class of mussel has a near annual turnover rate[15,42]. Therefore, these samples should integrate approximately annual variability in water mass signals. The adductor tissue was carefully dissected from all other tissues, rinsed with deionized water, refrozen, and then freeze-dried for 24 to 48 h; the remaining soft tissue parts were discarded. Based on the first year of sampling in 2010, within site isotopic variability was found to be narrow for $\delta^{13}C$ (average SD = ± 0.3‰) and $\delta^{15}N$ (average SD = ± 0.3‰)[13,14] therefore for subsequent sampling years, composites were prepared instead. Composites of mussel adductor tissue ($n = 5$) were then homogenized into a powder using a mortar and pestle and ~0.5–1.0 mg weighed into tin capsules for bulk isotope analysis.

Bulk stable isotope analysis

Stable isotopes of carbon ($\delta^{13}C$) and nitrogen ($\delta^{15}N$) were measured by the University of California Santa Cruz Stable Isotope Laboratory (UCSC-SIL) using a CE Instruments NC2500 elemental analyzer coupled to a Thermo Scientific DELTAplus XP isotope ratio mass spectrometer via a Thermo-Scientific Conflo III. For high C content samples, automated in line CO_2 trapping is used to remove interference with N_2. Isotopes values are reported using delta (δ) notation: $\delta^{13}C$ or $\delta^{15}N = [(R_{sample}/R_{standard}) - 1] \times 1000$, where R is the ratio of rare to common isotope of the sample (R_{sample}) and standard ($R_{standard}$), respectively, and corrected to VPDB (Vienna PeeDee Belemnite) for $\delta^{13}C$ and AIR for $\delta^{15}N$ against an in-house gelatin standard reference material (PUGel; ($\delta^{13}C = -12.6‰$, $\delta^{15}N = 5.6‰$) which is extensively calibrated against international standard reference materials. Measurements are corrected for size effects, blank-mixing effects, and drift effects. An externally-calibrated Acetanilide standard reference material ($\delta^{13}C = -29.5‰$, $\delta^{15}N = 1.1‰$) purchased from Dr. Arndt Schimmelmann of Indiana University is measured as a sample for independent quality control. Typical isotope ratio precision (1σ) is $< 0.1‰$ VPDB for $\delta^{13}C$ and $< 0.2‰$ AIR for $\delta^{15}N$.

Coupled physical–biogeochemical model

Physical properties of the regional circulation (temperature, salinity, ocean currents) were generated using an implementation of the Regional Ocean Modeling System (ROMS)[43,44] for the California Current System with a horizontal resolution of 1/30° (~3 km) and 42 vertical terrain-following levels. Biogeochemical properties were generated using NEMUCSC, which is a customized version of the North Pacific Ecosystem Model for Understanding Regional Oceanography (NEMURO) of Kishi et al.[45]. NEMUCSC includes three limiting macronutrients (nitrate, ammonium, and silicic acid), two phytoplankton functional groups (nanophytoplankton and diatoms), three zooplankton size-classes (microzooplankton, copepods, and euphausiids), and three detritus pools (dissolved and particulate organic nitrogen and particulate silica). In its current version, NEMUCSC also simulates carbon and oxygen cycling following the formulations of Hauri et al.[46] and Fennel et al.[47], respectively.

The model fields analyzed here are from a 26-year hindcast (1995–2020) of ROMS-NEMUCSC encompassing 30–48 N. ROMS is forced at the surface with atmospheric fields from the ERA5 reanalysis1 and at the model open ocean boundaries by the GLORYS global reanalysis2. NEMUCSC is similarly forced by daily averaged shortwave solar radiation from ERA5 and the GLORYS global hindcast3 for nutrients and dissolved oxygen at the open ocean boundaries. Additional details on the ROMS-NEMUCSC configuration and evaluation can be found in Fiechter et al.[3], Cheresh and Fiechter[4], Fiechter et al.[48], and Cheresh et al.[49].

Additional datasets

In addition to the mussel stable isotope data and ROMS-NEMUCSC model output, several other datasets were used in our analyses. Bathymetric data was extracted from the GEBCO 2022 grid (GEBCO Compilation Group, 2022). Monthly satellite chlorophyll-a (Chl-a) observations over our study domain from the E.U. Copernicus Marine Service Information GlobColour data product were accessed using the Copernicus Marine Toolbox Python API (E.U. Copernicus Marine Service Information, 2023). Monthly Pacific Decadal Oscillation (PDO) index data was accessed from the NOAA National Centers for Environmental Information website[50,51]. Monthly Oceanic Nino Index (ONI) and North Pacific Gyre Oscillation (NPGO) data were accessed from the NOAA Physical Sciences Laboratory website[8,52,53].

Data processing and statistical analyses

Data processing

Initial model output processing was completed using Ferret (https://ferret.pmel.noaa.gov/Ferret). All other data processing was done in Python using the pandas and xarray libraries, and data visualization was done using the cartopy, matplotlib and seaborn libraries. For the ROMS-NEMUCSC output, we calculated nearshore annual mean upwelling season (May to August) vertical velocity at 20 m depth, surface temperature, bottom temperature, surface nitrate, and bottom nitrate. For a given latitude, surface variables represent mean surface ocean values between 0 and 30 km from shore, and bottom variables represent values on the 100 m isobath, as indicative of upwelled source water properties. Continental shelf width was computed from the GEBCO 2022[54] bathymetry grid as the minimum distance between the 100 m isobath and the nearest point on the 0 m isobath to a given mussel collection site. Mean upwelling season (May to August) Chl-a concentrations from the GlobColour[55] data product were averaged over grid cells within 15 km from each study site. For several collection sites located near San Francisco Bay, only grid cell locations outside the Golden Gate were included. To facilitate direct comparison of the isotopic and other oceanographic datasets, we selected corresponding model output, shelf width and satellite Chl-a data from the same locations as the mussel collection sites.

Statistical data analysis

To assess environmental drivers of isotopic variability, we examined Spearman correlation coefficients between mussel tissue $\delta^{13}C$ and $\delta^{15}N$ values and oceanographic data transformed using Principal Component Analysis (PCA). Dimension reduction with PCA was done because many of the explanatory oceanographic variables used in our analyses exhibit multicollinearity. While regression coefficients and partial regression coefficients from multiple linear regression can help characterize the explanatory power of specific independent variables, independence of those explanatory variables is an important assumption. This assumption is often not met in complex systems. Indeed, correlation analysis shows strong relationships among explanatory variables in our datasets (Figs. S2, S3). In such cases, PCA is a useful approach to transform data into fully independent components that reflect shared variance among multiple predictors[56].

PCA was completed using the Python library scikit-learn, and Spearman correlation coefficients were computed using the SciPy library. All predictor variables were standardized (z-scored) before PCA analysis, to

ensure equal variances, and avoid biasing the PCA results depending on the units and variance of individual predictor variables. We performed two separate analyses to independently assess drivers of spatial and temporal isotopic variability. For the spatial analysis, only mean isotopic and oceanographic variable values at each study site were included. Explanatory variables for the spatial analysis include: vertical velocity at 20 m depth, surface temperature, bottom temperature, surface minus bottom temperature, surface nitrate concentrations, and bottom nitrate concentrations from the ROMS-NEMUCSC output, satellite Chl-a, continental shelf width and latitude. For the analysis of variability through time, only interannual anomalies (meaning the difference between mean annual values and the mean of all years) at each study site were included. The same explanatory variables listed above for the spatial analysis were used, except for the time-invariant variables shelf width and latitude. We report results for relationships between isotope variables and temporal PC1 and PC2 from the three different regions (north, central and south) separately, to emphasize regional differences in drivers of isotopic variability. However, the temporal PCA was trained using interannual anomalies sites from all three regions, so reported loadings are the same in all regions.

We also examined Spearman correlations between the climate indices (PDO, NPGO, ONI) and the isotopic and oceanographic variables. Climate indices were not included in the PCA analyses because they do not vary spatially, which would create redundancy due to input of the same time series at all locations.

Data availability

All datasets and code required to reproduce our main figures and analyses will be provided in a publicly available GitHub repository and archived using Zenodo prior to publication. The datasets on chlorophyll-a, climate indices and bathymetry are publicly available at: https://data.marine.copernicus.eu/product/OCEANCOLOUR_GLO_BGC_L4_MY_009_104/description; https://www.bodc.ac.uk/data/published_data_library/catalogue/10.5285/e0f0bb80-ab44-2739-e053-6c86abc0289c/; https://www.ncei.noaa.gov/pub/data/cmb/ersst/v5/index/ersst.v5.pdo.dat; https://www.psl.noaa.gov/data/correlation/npgo.data; https://psl.noaa.gov/data/correlation/oni.data. The bulk isotope data are available within the Supplementary Information files. Should any raw data files be needed in another format they are available from the corresponding author upon reasonable request.

Received: 20 July 2024; Accepted: 5 December 2024
Published online: 28 December 2024

References

1. Hickey, B. M. The California current system—hypotheses and facts. *Prog. Oceanogr.* **8**, 191–279 (1979).
2. Douglass, E., Roemmich, D. & Stammer, D. Interannual variability in northeast Pacific circulation. *J. Geophys. Res. Oceans* **111**, C04001 (2006).
3. Fiechter, J., Edwards, C. A. & Moore, A. M. Wind, circulation, and topographic effects on alongshore phytoplankton variability in the California current. *Geophys. Res. Lett.* **45**, 3238–3245 (2018).
4. Cheresh, J. & Fiechter, J. Physical and biogeochemical drivers of alongshore pH and oxygen variability in the California current system. *Geophys. Res. Lett.* **47**, e2020089553 (2020).
5. Checkley, D. M. & Barth, J. A. Patterns and processes in the California current system. *Prog. Oceanogr.* **83**(1), 49–64 (2009).
6. McPhaden, M. J., Zebiak, S. E. & Glantz, M. H. ENSO as an integrating concept in earth science. *Science* **314**(5806), 1740–1745 (2006).
7. Mantua, N. J. & Hare, S. R. The Pacific decadal oscillation. *J. Oceanogr.* **58**(1), 35–44 (2002).
8. Di Lorenzo, E. et al. North Pacific Gyre Oscillation links ocean climate and ecosystem change. *Geophys. Res. Lett.* **35**(8), L08607 (2008).
9. Jacox, M. G., Fiechter, J., Moore, A. M. & Edwards, C. A. ENSO and the California current coastal upwelling response. *J. Geophys. Res. Oceans* **120**, 1691–1702 (2015).
10. Graham, B. S., Koch, P. L., Newsome, S. D., McMahon, K. W. & Aurioles, D. Using isoscapes to trace the movements and foraging behavior of top predators in oceanic ecosystems. In *Isoscapes: Understanding Movement, Pattern, and Process on Earth through Isotope Mapping* (eds West, J. et al.) 299–318 (Springer, 2010).
11. McMahon, K. W., Hamady, L. L. & Thorrold, S. R. A review of ecogeochemistry approaches to estimating movements of marine animals. *Limnol. Oceanogr.* **58**(2), 697–714 (2013).
12. Kurle, C. M. & McWhorter, J. K. Spatial and temporal variability within marine isoscapes: implications for interpreting stable isotope data from marine systems. *Mar. Ecol. Prog. Ser.* **568**, 31–45 (2017).
13. Vokhshoori, N. L., Larsen, T. & McCarthy, M. D. Reconstructing $\delta^{13}C$ isoscapes of phytoplankton production in a coastal upwelling system with amino acid isotope values of littoral mussels. *Mar. Ecol. Prog. Ser.* **504**, 59–72 (2014).
14. Vokhshoori, N. L. & McCarthy, M. D. Compound-specific $\delta^{15}N$ amino acid measurements in littoral mussels in the California upwelling ecosystem: a new approach to generating baseline $\delta^{15}N$ isoscapes for coastal ecosystems. *PLoS ONE* **9**, e98087 (2014).
15. Vokhshoori, N. L., Tipple, B. T., Teague, L., Bailess, A. & McCarthy, M. D. Calibrating bulk and amino acid $\delta^{13}C$ and $\delta^{15}N$ isotope ratios between bivalve soft tissue and shell for paleoecological reconstructions. *Palaeogeogr. Palaeoclimatol. Palaeoecol.* **595**, 110979 (2022).
16. Rodríguez-Pérez, M. Y. et al. $\delta^{13}C$ and $\delta^{15}N$ zooplankton isoscapes as trace of water masses and mesoscale activity in the Pacific Tropical-Subtropical Convergence off Mexico during June 2010. *Sci. Total Environ.* **909**, 168497 (2024).
17. Rau, G. H., Chavez, F. P. & Friederich, G. E. Plankton $^{13}C/^{12}C$ variations in Monterey Bay, California: evidence of non-diffusive inorganic carbon uptake by phytoplankton in an upwelling environment. *Deep Sea Res. I* **48**, 79–94 (2001).
18. Mackensen, A. & Schmiedl, G. Stable carbon isotopes in paleoceanography: atmosphere, oceans, and sediments. *Earth Sci. Rev.* **197**, 102893 (2019).
19. Wilkes, E. B. & Pearson, A. A general model for carbon isotopes in red-lineage phytoplankton: interplay between unidirectional processes and fractionation by RubisCO. *Geochim. Cosmochim. Acta* **265**, 163–181 (2019).
20. Bograd, S. J., Schroeder, I. D. & Jacox, M. G. A water mass history of the Southern California current system. *Geophys. Res. Lett.* **46**, 6690–6698 (2019).
21. Voss, M., Dippner, J. W. & Montoya, J. P. Nitrogen isotope patterns in the oxygen-deficient waters of the Eastern Tropical North Pacific Ocean. *Deep Sea Res. I* **48**, 1905–1921 (2001).
22. Sigman, D. M., Kash, K. L. & Casciotti, K. L. Ocean process tracers: nitrogen isotopes in the ocean. In *Encyclopedia of Ocean Science*, 2nd edn. (Elsevier, 2009).

23. Altabet, M. A. et al. The nitrogen isotope biogeochemistry of sinking particles from the margin of the Eastern North Pacific. *Deep Sea Res. I* **46**, 655–679 (1999).
24. Biller, D. V., Coale, T. H., Till, R. C., Smith, G. J. & Bruland, K. W. Coastal iron and nitrate distributions during the spring and summer upwelling season in the central California Current upwelling regime. *Cont. Shelf Res.* **66**, 58–72 (2013).
25. Messié, M. & Chavez, F. Seasonal regulation of primary production in eastern boundary upwelling systems. *Prog. Oceanogr.* **134**, 1–18 (2015).
26. Sigman, D. M. & Fripiat, F. Nitrogen isotopes in the ocean. In *Encyclopedia of Ocean Sciences* (eds Cochran, J. K. et al.) 3 edn, 263–278 (Academic, 2019).
27. Ek, C., Karlson, A. M. L., Hansson, S., Garbaras, A. & Gorokhova, E. Stable isotope composition in daphnia is modulated by growth, temperature, and toxic exposure: implications for trophic magnification factor assessment. *Environ. Sci. Technol.* **49**, 6934–6942 (2015).
28. Lienart, C. et al. Karlsson. Long- term changes in trophic ecology of blue mussels in a rapidly changing ecosystem. *Limnol. Oceanogr.* **66**, 694–710 (2020).
29. Letendre, J., Manduzio, H., Bultelle, M. M., Leboulenger, F. & Durand, F. Tidal height influences the levels of enzymatic antioxidant defences in *Mytilus edulis*. *Mar. Environ. Res.* **67**, 69–74 (2009).
30. Lesser, M. Climate change stressors cause metabolic depression in the blue mussel, *Mytilus edulis*, from the Gulf of Maine. *Limnol. Oceanogr.* **61**(5), 1705–1717 (2016).
31. McCabe, R. M. et al. An unprecedented coastwide toxic algal bloom linked to anomalous ocean conditions. *Geophys. Res. Lett.* **43**, 10366–10376 (2016).
32. Fiechter, J. & Moore, A. M. Physical and biogeochemical properties of California current upwelled source waters. *J. Geophys. Res. Oceans* **129**, e2023JC020164 (2024).
33. Rosenfeld, L. K., Schwing, F. B., Garfield, N. & Tracy, D. E. Bifurcated flow from an upwelling center—A cold-water source for Monterey Bay. *Cont. Shelf Res.* **14**, 931–964 (1994).
34. Wilkerson, F. P., Dugdale, R. C., Kudela, R. M. & Chavez, F. P. Biomass and productivity in Monterey Bay, California: contribution of the large phytoplankton. *Deep Sea Res. II* **47**, 1003–1022 (2000).
35. Graham, W. M. & Largier, J. L. Upwelling shadows as nearshore retention sites: the example of northern Monterey Bay. *Cont. Shelf Res.* **17**, 509–532 (1997).
36. Chavez, F. P. & Messié, M. A comparison of eastern boundary upwelling ecosystems. *Prog. Oceanogr.* **83**, 80–96 (2009).
37. Ware, D. M. & Thompson, R. E. Bottom-up ecosystem trophic dynamics determine fish production in the northeast Pacific. *Science* **308**, 1280–1284 (2005).
38. Chase, Z., Strutton, P. G. & Hales, B. Iron links river runoff and shelf width to phytoplankton biomass along the U.S. West Coast. *Geophys. Res. Lett.* **34**, L04607 (2007).
39. Jacox, M. G. & Edwards, C. A. Effects of stratification and shelf slope on nutrient supply in coastal upwelling regions. *J. Geophys. Res. Oceans* **116**, C03019 (2011).
40. Jacox, M. G. et al. Impacts of the 2015–2016 El Niño on the California Current System: early assessment and comparison to past events. *Geophys. Res. Lett.* **43**, 7072–7080 (2016).
41. Ryan, J. P. et al. Causality of an extreme harmful algal bloom in Monterey Bay, California, during the 2014–2016 northeast Pacific warm anomaly. *Geophys. Res. Lett.* **44**, 5571–5579 (2017).
42. Gorokhova, E. & Hansson, S. An experimental study on variations in stable carbon and nitrogen isotope fractionation during growth of Mysis mixta and Neomysis integer. *Can. J. Fish. Aquat. Sci.* **56**, 2203–2210 (1999).
43. Shchepetkin, A. F. & McWilliams, J. C. The regional oceanic modeling system (ROMS): a split-explicit, free-surface, topography-following-coordinate oceanic model. *Ocean Model.* **9**(4), 347–404 (2005).
44. Haidvogel, D. B. et al. Ocean forecasting in terrain-following coordinates: Formulation and skill assessment of the Regional Ocean modeling system. *J. Comput. Phys.* **227**(7), 3595–3624 (2008).
45. Kishi, M. J. et al. NEMURO—a lower trophic level model for the North Pacific Marine ecosystem. *Ecol. Model.* **202**, 12–25 (2007).
46. Hauri, C., Gruber, N., McDonnell, A. M. P. & Vogt, M. The intensity, duration, and severity of low aragonite saturation state events on the California continental shelf. *Geophys. Res. Lett.* **40**, 3424–3428 (2013).
47. Fennel, K., Wilkin, J., Previdi, M. & Najjar, R. Denitrification effects on air-sea CO2 flux in the coastal ocean: simulations for the northwest North Atlantic. *Geophys. Res. Lett.* **35**, 24 (2008).
48. Fiechter, J., Santora, J. A., Chavez, F., Northcott, D. & Messié, M. Krill hotspot formation and phenology in the California current ecosystem. *Geophys. Res. Lett.* **47**, e2020088039 (2020).
49. Cheresh, J., Kroeker, K. J. & Fiechter, J. Upwelling intensity and source water properties drive high interannual variability of corrosive events in the California Current. *Sci. Rep.* **13**(1), 13013 (2023).
50. Mantua, N. J., Hare, S. R., Zhang, Y., Wallace, J. M. & Francis, R. C. A Pacific interdecadal climate oscillation with impacts on salmon production. *Bull. Am. Meteorol. Soc.* **78**(6), 1069–1079 (1997).
51. NOAA National Centers for Environmental Information. *Pacific Decadal Oscillation*. https://www.ncei.noaa.gov/pub/data/cmb/ersst/v5/index/ersst.v5.pdo.dat (2023).
52. NOAA Physical Sciences Laboratory. *North Pacific Gyre Oscillation*. https://www.psl.noaa.gov/data/correlation/npgo.data (2023).
53. NOAA Physical Sciences Laboratory. *Oceanic Niño Index*. https://psl.noaa.gov/data/correlation/oni.data (2023).
54. GEBCO Compilation Group. *GEBCO 2022 Grid*. https://doi.org/10.5285/e0f0bb80-ab44-2739-e053-6c86abc0289c (2022).
55. E.U. Copernicus Marine Service Information. *Global Ocean Colour (Copernicus-GlobColour), Bio-Geo-Chemical, L4 (Monthly and Interpolated) from Satellite Observations*. https://doi.org/10.48670/moi-00281 (2023).
56. Graham, M. H. Confronting multicollinearity in ecological multiple regression. *Ecology* **84**, 2809–2815 (2003).

Acknowledgements

Deep appreciation is extended to the many field assistants who helped in the sample collection over the years: Nadine Quintana Krupinski, Liz Browne, Mark Holland, Nikolas Vokhshoori, Melody Overstreet and Laurel Teague. We thank UC Santa Cruz's Stable Isotope Lab staff, Dyke Andresen and Colin Carney for assistance in bulk isotope analysis. This study was in part supported by National Science Foundation (BCS 2115145 to M.D.M).

Author contributions

All individuals listed have agreed to be authors, approve of the submitted version of the manuscript and have made significant contributions to the manuscript. NLV and MDM originally formulated the idea. NLV developed the methodology did the sampling, sample processing, and generated bulk isotope data. JF generated the model output. GP performed most of the statistical analyses and generated the figures, NLV contributed. NLV wrote the manuscript; other authors provided detailed editorial advice.

Declarations

Competing interests
The authors declare no competing interests.

Additional information
Supplementary Information The online version contains supplementary material available at https://doi.org/10.1038/s41598-024-82457-w.

Correspondence and requests for materials should be addressed to N.L.V.

Reprints and permissions information is available at www.nature.com/reprints.

Publisher's note Springer Nature remains neutral with regard to jurisdictional claims in published maps and institutional affiliations.